Available online at www.sciencedirect.com

ScienceDirect

Nuclear Physics B 941 (2019) 744–754

NUCLEAR PHYSICS B

www.elsevier.com/locate/nuclphysb

A two loop radiative neutrino model

Seungwon Baek [a], Hiroshi Okada [b,*], Yuta Orikasa [c]

[a] *Department of Physics, Korea University, Seoul 02841, Republic of Korea*
[b] *Asia Pacific Center for Theoretical Physics, Pohang, Gyeongbuk 790-784, Republic of Korea*
[c] *Institute of Experimental and Applied Physics, Czech Technical University, Prague 12800, Czech Republic*

Received 17 January 2018; received in revised form 4 February 2019; accepted 3 March 2019
Available online 7 March 2019
Editor: Hong-Jian He

Abstract

We explore the possibility to explain a bosonic dark matter candidate with a gauge singlet inside the loop to generate the neutrino mass matrix at two-loop level. The mass matrix is suppressed by a small mixing that comes from the bound on direct detection experiments of the dark matter, and equivalent of the three-loop neutrino model due to the small mixing between neutral inert bosons. Here, our setup is the Zee-Babu type scenario with Z_3 discrete symmetry, in which we consider the neutrino oscillation data, lepton flavor violations, muon $g-2$, $\mu-e$ conversion rate, lepton flavor-changing and conserving Z boson decay and bosonic dark matter candidate.

1. Introduction

Radiatively induced neutrino masses is one of the promising scenarios which make strong correlations between neutrinos and any fields that are introduced inside loops. If a dark matter (DM) candidate is introduced in the model, its testability is enhanced due to the fact that parameter space is strongly constrained by neutrino data. Especially two-loop induced models that we will focus on in this paper have been widely studied in various aspects [1–34].

* Corresponding author.
E-mail addresses: sbaek@korea.ac.kr (S. Baek), hiroshi.okada@apctp.org (H. Okada), Yuta.Orikasa@utef.cvut.cz (Y. Orikasa).

https://doi.org/10.1016/j.nuclphysb.2019.03.002

Table 1
Particle contents and charge assignments of leptons and new particles under $SU(2)_L \times U(1)_Y \times Z_3$. Here $\omega \equiv e^{2\pi i/3}$.

	Lepton fields			Scalar fields			
	L_L	e_R	$N_{L/R}$	Φ	η	χ	χ^+
$SU(2)_L$	**2**	**1**	**1**	**2**	**2**	**1**	**1**
$U(1)_Y$	$-\frac{1}{2}$	-1	0	$\frac{1}{2}$	$\frac{1}{2}$	0	1
Z_3	1	1	ω	1	ω	ω	ω

In this paper, we study the muon anomalous magnetic moment, various lepton flavor violations (LFVs), and DM phenomenology in the framework of Zee-Babu type of neutrino model, emphasizing $\mu - e$ conversion rate in $Titanium$ nuclei that will be tested in the near future experiment such as PRISM/PRIME [35]. Despite a two-loop model, we will also show that the scale of neutrino mass in our model is equivalent to a three-loop model. It is due to the small mixing between neutral bosons dictated by the direct detection bound of the DM candidate.

This paper is organized as follows. In Sec. 2, we introduce our model, including neutrino sector, LFVs, muon anomalous magnetic moment and lepton flavor-changing and conserving Z boson decay. In Sec. 3, we present our numerical analysis and identify regions consistent with the current experiments. We conclude and discuss in Sec. 4.

2. Model setup

We introduce three families of iso-spin singlet vector-like neutral fermions N_i $(i = 1, 2, 3)$, iso-spin doublet scalar η, an isospin singlet neutral scalar χ and charged scalars $\chi^\pm$ in addition to the SM fields. We impose a discrete Z_3 symmetry on all the new particles $(N, \eta, \chi, \chi^\pm)$ in order to assure the stability of DM (χ in our case). The particle contents and their charge assignments under $SU(2)_L \times U(1)_Y \times Z_3$ are shown in Table 1.[1] Thus we expect that only the SM-like Higgs Φ has a vacuum expectation value (VEV), which is denoted by $\langle \Phi^0 \rangle = v/\sqrt{2}$ [21]. Then the relevant Lagrangian and scalar potential respecting the symmetries are given by

$$\begin{aligned}
-\mathcal{L}_Y &= (y_\ell)_{ij} \bar{L}_{L_i} \Phi e_{R_j} + (y_\eta)_{ij} \bar{L}_{L_i} (i\sigma_2) \eta^* N_{R_j} + y_{N_{R_{ij}}} \bar{N}^c_{R_i} N_{R_j} \chi + y_{N_{L_{ij}}} \bar{N}^c_{L_i} N_{L_j} \chi \\
&\quad + (y_\chi)_{ij} \bar{N}_{L_i} e_{R_j} \chi^+ + M_{N_i} \bar{N}_{L_i} N_{R_i} + \text{h.c.}, \qquad (2.1) \\
\mathcal{V} &= m_\Phi^2 \Phi^\dagger \Phi + m_\eta^2 |\eta|^2 + m_\chi^2 |\chi|^2 + m_{\chi^\pm}^2 |\chi^+|^2 \\
&\quad + \mu (\eta^T (i\sigma_2) \Phi \chi^- + \text{h.c.}) + \mu_{\eta\chi} (\Phi^\dagger \eta \chi^* + \text{h.c.}) + \mu_\chi (\chi^3 + \text{h.c.}) \\
&\quad + \lambda_\Phi (\Phi^\dagger \Phi)^2 + \lambda_0 (\Phi^\dagger \eta \chi^2 + \text{h.c.}) + \lambda_\eta (\eta^\dagger \eta)^2 + \lambda_\chi (\chi^* \chi)^2 + \lambda_{\chi^\pm} (\chi^+ \chi^-)^2 \\
&\quad + \lambda_{\Phi\eta} (\Phi^\dagger \Phi)(\eta^\dagger \eta) + \lambda'_{\Phi\eta} |\Phi^\dagger \eta|^2 + \lambda_{\Phi\chi} (\Phi^\dagger \Phi) \chi^* \chi + \lambda_{\eta\chi} (\eta^\dagger \eta) \chi^* \chi \\
&\quad + \lambda_{\Phi\chi^\pm} (\Phi^\dagger \Phi) \chi^+ \chi^- + \lambda_{\eta\chi^\pm} (\eta^\dagger \eta) \chi^+ \chi^- + \lambda_{\chi\chi^\pm} (\chi^* \chi) \chi^+ \chi^-, \qquad (2.2)
\end{aligned}$$

where σ_2 is the second Pauli matrix, $i, j = 1 - 3$, and the first term of $\mathcal{L}_Y$ can generate the SM charged-lepton masses $m_\ell \equiv y_\ell v/\sqrt{2}$ $(\ell = 1 - 3)$ after the electroweak symmetry breaking. Both N_i and e_i can be considered as the mass eigenstates without loss of generality. For simplicity we assume all the parameters in (2.1) are real and positive.

[1] Although there are many other possible symmetries to realize our model, Z_3 is a minimal symmetry.

The scalar fields can be parameterized as follows:

$$\Phi = \begin{bmatrix} 0 \\ \frac{v+\phi}{\sqrt{2}} \end{bmatrix}, \quad \eta = \begin{bmatrix} \eta^+ \\ \eta^0 \end{bmatrix}, \quad \chi, \quad \chi^\pm, \tag{2.3}$$

where η^0 and χ are complex inert neutral bosons, $\eta^\pm$ and $\chi^\pm$ are the singly charged bosons, $v \simeq 246$ GeV is VEV of the Higgs doublet, and ϕ is the SM Higgs boson with mass $m_\phi \approx 125.5$ GeV. To ensure the stability of DM, the following condition should be at least satisfied:

$$|\,\mu + \mu_{\eta\chi} + \mu_\chi\,| < \sqrt{\Lambda}(m_\Phi^2 + m_\eta^2 + m_\chi^2 + m_{\chi^\pm}^2)^{\frac{1}{2}}, \ \Lambda \equiv \sum_{\text{i=all quartic couplings}} \lambda_i. \tag{2.4}$$

Notice here that we have mixing between inert bosons through $\mu_{\eta\chi}$ and μ, the resulting mass eigenvalues and their rotation matrices are obtained by

$$O_H^T M_H O_H = \begin{bmatrix} m_{H_1} & 0 \\ 0 & m_{H_2} \end{bmatrix}, \quad \begin{bmatrix} \chi \\ \eta^0 \end{bmatrix} = O_H \begin{bmatrix} H_1 \\ H_2 \end{bmatrix} = \begin{bmatrix} \cos\alpha & \sin\alpha \\ -\sin\alpha & \cos\alpha \end{bmatrix} \begin{bmatrix} H_1 \\ H_2 \end{bmatrix}, \tag{2.5}$$

$$V_C^T M_{H^\pm} V_C = \begin{bmatrix} m_{H_1^\pm} & 0 \\ 0 & m_{H_2^\pm} \end{bmatrix}, \quad \begin{bmatrix} \chi^\pm \\ \eta^\pm \end{bmatrix} = V_C \begin{bmatrix} H_1^\pm \\ H_2^\pm \end{bmatrix} = \begin{bmatrix} \cos\beta & \sin\beta \\ -\sin\beta & \cos\beta \end{bmatrix} \begin{bmatrix} H_1^\pm \\ H_2^\pm \end{bmatrix}, \tag{2.6}$$

where $(H_{1(2)}, H_{1(2)}^\pm)$ and (α, β) can be written in terms of the parameters in the scalar potential, and we use the short hand notation $s_{\alpha(\beta)}$ and $c_{\alpha(\beta)}$ for $\sin\alpha(\beta)$ and $\cos\alpha(\beta)$ below.[2]

DM candidate: The lightest neutral scalar H_1 is our DM candidate. Here we consider constraints on H_1. As for the direct detection experiment, the dominant elastic scattering cross section comes from Z-boson portal through mixing and found as

$$\sigma_{SI} \simeq \left(\frac{m_{H_1} m_p}{m_{H_1} + m_p}\right)^2 \frac{2G_F^2 s_\alpha^4}{\pi} \left(1 - 4s_w^2\right)^2, \tag{2.7}$$

where m_p is a proton mass, $s_w^2 \approx 0.23$ is the Weinberg angle and G_F is the Fermi constant. Note here that s_α^4 comes from the kinetic term of η, $D_\mu \eta^\dagger D_\mu \eta$, where the covariant derivative D_μ includes the SM gauge boson Z. Since Z-boson couples only to the isospin doublet scalar, in the effective $H_1 - H_1 - Z$ coupling only η component of H_1 couples to Z-boson. This leads to s_α^2 suppression in the effective coupling and s_α^4 suppression in the cross section for the DM scattering off the nuclei. In the experiment of LUX [36], the typical upper bound on the cross section is $\sigma_{SI} \lesssim 10^{-45}$ cm^2 at $m_{H_1} = \mathcal{O}(100)$ GeV. Then the required condition on α is given by[3]

$$|s_\alpha| \lesssim 5 \times 10^{-2}. \tag{2.8}$$

It implies that the dominant component of the DM candidate is the gauge singlet boson χ. Hereafter we will neglect any terms proportional to s_α^4. To explain the relic density, we rely on the resonant effect via s-channel of the SM-Higgs, and we consider only the annihilation processes,

[2] See ref. [21] for scalar mass spectra in more details.

[3] If we consider the contribution of the Higgs portal [37,39] to the direct detection, the constraint is given by $2\lambda_{\Phi\chi} c_\alpha^2 - 2\frac{\mu_{\eta\chi}}{v} s_\alpha c_\alpha + (\lambda_{\Phi\eta} + \lambda'_{\Phi\eta}) s_\alpha^2 \lesssim 10^{-2}$. Thus one can satisfy the bound of direct detection by tuning the Higgs trilinear and quartic couplings.

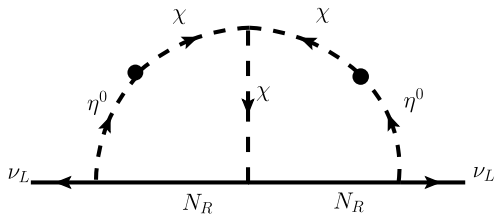

Fig. 1. Two-loop diagram to induce neutrino mass matrix. Here the blobs indicate the scalar mixing between η^0 and χ.

since our DM is gauge singlet.[4] In this case, to satisfy the relic density $\Omega h^2 \approx 0.12$, the DM mass should be around the Higgs resonance region $m_{H_1} \approx m_\phi/2 \approx 63$ GeV [39].

2.1. Neutrino masses

The active neutrino mass matrix m_ν is generated at two-loop level as shown in Fig. 1, and its formula is given by

$$(m_\nu)_{ij} = \frac{12\sqrt{2}\mu_\chi s_\alpha^2 c_\alpha^2 (y_\eta)_{ia}(y_N)_{ab}(y_\eta)^T_{bj}}{(4\pi)^4} F_{II} \equiv (y_\eta)_{ia}(R_N)_{ab}(y_\eta)^T_{bj}, \tag{2.9}$$

$$F_{II} = \int \frac{[dx]}{z-1}\int [da]\left[c_\alpha^2\left[\ln\left(\frac{\Delta_{111}}{\Delta_{112}}\right) - \ln\left(\frac{\Delta_{211}}{\Delta_{212}}\right)\right] + s_\alpha^2\left[\ln\left(\frac{\Delta_{222}}{\Delta_{221}}\right) - \ln\left(\frac{\Delta_{122}}{\Delta_{121}}\right)\right]\right], \tag{2.10}$$

$$\Delta_{\ell mn} = -a\frac{xM_{N_b}^2 + ym_{H_n}^2 + zm_{H_m}^2}{z^2 - z} + bM_{N_a}^2 + cm_{H_\ell}^2, \tag{2.11}$$

where R_N is a parameter with a mass dimension and depends on the parameters $(y_N, \mu_\chi, s_\alpha, F_{II})$, $[dx] \equiv dx\,dy\,dz\,\delta(x+y+z-1)$, $[da] \equiv da\,db\,dc\,\delta(a+b+c-1)$, and we assume $y_N \equiv y_{N_R} \approx y_{N_L}$. As we mentioned in Section 1, although they are generated at two-loop level, the neutrino masses scale like three-loop model due to s_α suppression. Then the active neutrino mass matrix $(m_\nu)_{ij}$ can be diagonalized by the Pontecorvo-Maki-Nakagawa-Sakata (PMNS) mixing matrix $V_{\rm MNS}$ [40] as

$$(m_\nu)_{ij} = (V^*_{\rm MNS} D_\nu V^\dagger_{\rm MNS})_{ij}, \quad D_\nu \equiv {\rm diag}(m_{\nu_1}, m_{\nu_2}, m_{\nu_3}), \tag{2.12}$$

$$V_{\rm MNS} = \begin{bmatrix} c_{13}c_{12} & c_{13}s_{12} & s_{13}e^{-i\delta} \\ -c_{23}s_{12} - s_{23}s_{13}c_{12}e^{i\delta} & c_{23}c_{12} - s_{23}s_{13}s_{12}e^{i\delta} & s_{23}c_{13} \\ s_{23}s_{12} - c_{23}s_{13}c_{12}e^{i\delta} & -s_{23}c_{12} - c_{23}s_{13}s_{12}e^{i\delta} & c_{23}c_{13} \end{bmatrix}. \tag{2.13}$$

We assume the neutrino masses are normal ordered, neglect the Majorana phases, and fix the Dirac phase $\delta = -\pi/2$ in the numerical analysis for simplicity. Then we apply the generalized Casas-Ibarra parametrization[5] to our analysis which use the observed neutrino oscillation data with global fit [41]. We impose $\sum_{i=1-3} m_{\nu_i} < 0.12$ eV at 95% C.L. as reported by Planck collaboration [42]. The Yukawa coupling y_η can be rewritten in terms of the following parameters:

[4] If our DM is dominated by $SU(2)_L$ gauge doublet, then coannihilation is important and the allowed mass is at around 535 GeV [38].

[5] In our case, the central matrix is not diagonal but the symmetric matrix which is proportional to y_N.

$$y_\eta \approx V^*_{\rm MNS}\sqrt{D_\nu}\mathcal{O}(\theta_i)\left(R_N{}^{Ch}\right)^{-1}, \tag{2.14}$$

where $\mathcal{O}(\theta_i)$ is an arbitrary orthogonal 3×3 matrix with three complex values θ_i (i=1-3) that satisfy $\mathcal{O}\mathcal{O}^T = \mathcal{O}^T\mathcal{O} = {\rm Diag}(1,1,1)$[6] and R_N^{Ch} is Cholesky decomposed matrix. This matrix is a lower triangular matrix and satisfies the following relation (see appendix A),

$$R_N = R_N^{Ch}\left(R_N^{Ch}\right)^T. \tag{2.15}$$

2.2. Lepton flavor violations and muon $(g-2)$

Lepton flavor violations (LFVs) at one-loop level arise from the terms with y_η and y_χ as shown in the left panel of Fig. 2.[7] Between two classes of LFV modes $\ell_i \to \ell_j\gamma$ and $\ell_i \to \ell_j\ell_k\ell_\ell$, the former tends to give more stringent bounds on the related couplings and masses [43]. Thus we consider only this mode below. The model prediction for the radiative decay channel in our case is given by

$${\rm BR}(\ell_i\to\ell_j\gamma) = \frac{48\pi^3 C_{ij}\alpha_{\rm em}}{{\rm G_F^2}}\left(|(a_R^{\eta\chi})_{ij} + a^\eta_{R_{ij}} + \epsilon_{ij}a^\chi_{R_{ij}}|^2 + |(a_L^{\eta\chi})_{ij} + \epsilon_{ij}a^\eta_{L_{ij}} + a^\chi_{L_{ij}}|^2\right), \tag{2.16}$$

$$(a_R^{\eta\chi})_{ij} = (a_L^{\eta\chi})^\dagger_{ij} = -\frac{s_\beta c_\beta}{(4\pi)^2}\sum_{k=1,2,3}\frac{M_{N_k}}{m_{\ell_i}}(y_\eta)_{jk}(y_\chi)_{ki}\left(F_1(M_{N_k},m_{H_1^\pm}) - F_1(M_{N_k},m_{H_2^\pm})\right), \tag{2.17}$$

$$a^\eta_{R_{ij}} = a^\eta_{L_{ij}} = \sum_{k=1,2,3}\frac{(y_\eta)_{jk}(y_\eta^\dagger)_{ki}}{(4\pi)^2}\left[s_\beta^2 F_{lfv}(M_{N_k},m_{H_1^\pm}) + c_\beta^2 F_{lfv}(M_{N_k},m_{H_2^\pm})\right], \tag{2.18}$$

$$a^\chi_{R_{ij}} = a^\chi_{L_{ij}} = \sum_{k=1,2,3}\frac{(y_\chi^\dagger)_{jk}(y_\chi)_{ki}}{(4\pi)^2}\left[c_\beta^2 F_{lfv}(M_{N_k},m_{H_1^\pm}) + s_\beta^2 F_{lfv}(M_{N_k},m_{H_2^\pm})\right], \tag{2.19}$$

$$F_1(m_1,m_2) = \frac{m_1^2+m_2^2}{2(m_1^2-m_2^2)^2} - \frac{m_1^2m_2^2}{(m_1^2-m_2^2)^3}\log\frac{m_1^2}{m_2^2}, \tag{2.20}$$

$$F_{lfv}(m_a,m_b) = \frac{2m_a^6+3m_a^4m_b^2-6m_a^2m_b^4+6m_b^6+12m_a^4m_b^2\ln(m_b/m_a)}{12(m_a^2-m_b^2)^4}, \tag{2.21}$$

where $\epsilon_{ij}\equiv(m_{\ell_j}/m_{\ell_i})(\ll 1)$, $\eta^\pm$ is the singly charged component of η, ${\rm G_F}\approx 1.17\times 10^{-5}$ [GeV]$^{-2}$ is the Fermi constant, $\alpha_{\rm em}\approx 1/137$ is the fine structure constant, $C_{21}\approx 1$, $C_{31}\approx 0.1784$, and $C_{32}\approx 0.1736$. Note that in the limit $m_{\ell_i}\to 0$ Eq. (2.17) is divergent, but this mass comes from the total decay rate and $m_{\ell_i}\to 0$ limit is unphysical. Experimental upper bounds are ${\rm BR}(\mu\to e\gamma)\lesssim 4.2\times 10^{-13}$, ${\rm BR}(\tau\to e\gamma)\lesssim 3.3\times 10^{-8}$, and ${\rm BR}(\tau\to\mu\gamma)\lesssim 4.4\times 10^{-8}$ [46,47].

[6] In case the family number of N_R is two, $\mathcal{O}(\theta)$ is an arbitrary 3×2 matrix with a complex value θ that satisfies $\mathcal{O}\mathcal{O}^T = {\rm Diag}(0,1,1)$ and $\mathcal{O}^T\mathcal{O} = {\rm Diag}(1,1)$. The numerical result for the three families does not change much from this case.

[7] Recently sophisticated analysis has been done by refs. [44,45].

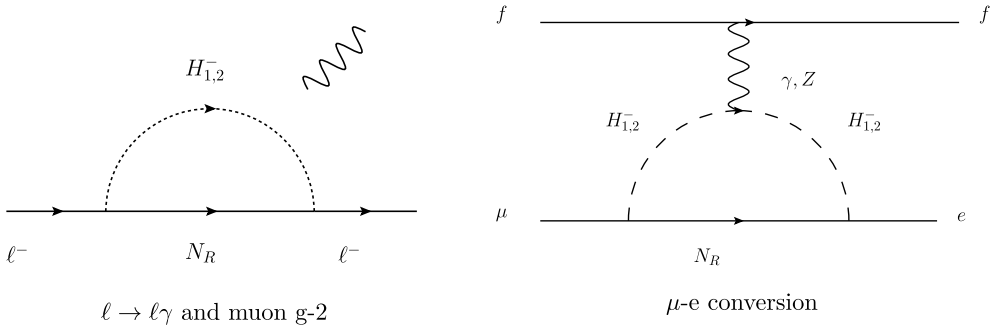

Fig. 2. LFV diagrams.

Table 2
Summary for the $\mu - e$ conversion in various nuclei: Z, $Z_{\rm eff}$, $F(q)$, $\Gamma_{\rm capt}$, and the bounds on the capture rate R.

Nucleus $^A_Z N$	$Z_{\rm eff}$	$\lvert F(-m_\mu^2)\rvert$	$\lvert\Gamma_{\rm capt}$ (10^6sec^{-1})	Experimental bound (Future bound)	$Y \equiv \frac{R}{\rm BR(\mu\to e\gamma)}$
$^{27}_{13}Al$	11.5	0.64	0.7054	($R_{Al} \lesssim 10^{-16}$) [50]	0.25
$^{48}_{22}Ti$	17.6	0.54	2.59	$R_{Ti} \lesssim 4.3 \times 10^{-12}$ [51] ($\lesssim 10^{-18}$ [35])	0.44
$^{197}_{79}Au$	33.5	0.16	13.07	$R_{Au} \lesssim 7 \times 10^{-13}$ [52]	0.36
$^{208}_{82}Pb$	34	0.15	13.45	$R_{Pb} \lesssim 4.6 \times 10^{-11}$ [53]	0.34

The $\mu - e$ *conversion* rate can be expressed by using $a_{R/L}$ defined in Eqs. (2.17), (2.18), and (2.19). The Feynman diagram is shown in the right panel of Fig. 2, and its capture rate R is obtained approximately to be[8]

$$\begin{aligned} R &\approx \frac{C_{\mu e}|Z|^2}{\Gamma_{\rm cap}}\left(|(a_R^{\eta\chi})_{\mu e} + a^{\eta}_{R_{\mu e}} + \epsilon_{\mu e} a^{\chi}_{R_{\mu e}}|^2 + |(a_L^{\eta\chi})_{\mu e} + \epsilon_{\mu e} a^{\eta}_{L_{\mu e}} + a^{\chi}_{L_{\mu e}}|^2\right), \\ C_{\mu e} &\approx 4\alpha_{\rm em}^5 \frac{Z_{\rm eff}^4 |F(q)|^2 m_\mu^5}{Z}, \end{aligned} \tag{2.22}$$

where Z, $Z_{\rm eff}$, $F(q)$, and R are given in Table 2.

Here let us define $Y \equiv \frac{R}{\rm BR(\mu\to e\gamma)}$, since their flavor structures are same. Then it is given by

$$Y \approx 1.22 \times 10^{-24} \left(\frac{Z Z_{\rm eff}^4 |F(q)|^2}{\Gamma_{\rm cap}}\right). \tag{2.23}$$

Depending on the nuclei, $Y \approx \mathcal{O}(0.1)$, as listed in Table 2. It suggests that the constraint from the $\mu - e$ conversion is always satisfied once we satisfy the constraint of $\mu \to e\gamma$. We will discuss the sensitivity of future experiments, R_{Ti} and R_{Al}, in the numerical analysis.

New contribution to the muon anomalous magnetic moment (muon $g-2$*)*, whose diagram is displayed in the left panel of Fig. 2, is given by

$$\Delta a_\mu \approx -m_\mu^2 [(a_R^{\eta\chi})_{\mu\mu} + a^{\eta}_{R_{\mu\mu}} + \epsilon_{\mu\mu} a^{\chi}_{R_{\mu\mu}} + (a_L^{\eta\chi})_{\mu\mu} + \epsilon_{\mu\mu} a^{\eta}_{L_{\mu\mu}} + a^{\chi}_{L_{\mu\mu}}], \tag{2.24}$$

[8] We neglect the contribution from the Z-penguin diagram due to suppression factor $(m_\ell/M_N)^2$.

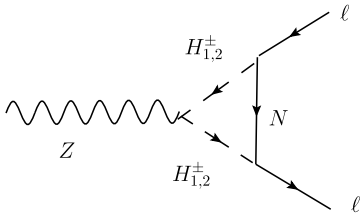

Fig. 3. The diagram for the lepton flavor-changing/conserving Z boson decay.

where only the terms $(a^{\eta\chi}_{R(L)})_{\mu\mu}$ are positive contributions to the muon $g-2$. Thus we expect $a^{\eta}_{R(L)_{\mu\mu}}, a^{\chi}_{R(L)_{\mu\mu}} \ll (a^{\eta\chi}_{R/L})_{\mu\mu}$ to explain the discrepancy between the experimental results and the theoretical predictions which is of order of $\mathcal{O}(10^{-9})$ [48].

Lepton Flavor-Changing/Conserving Z Boson Decay: Here, we consider the flavor changing/conserving Z boson decay $Z \to \ell_i^- \ell_j^+$ as shown in Fig. 3, whose branching fractions have been measured or restricted by experiments as [46],

$$\mathrm{BR}(Z \to e^- e^+) = (3.363 \pm 0.004)\%, \tag{2.25}$$

$$\mathrm{BR}(Z \to \mu^- \mu^+) = (3.366 \pm 0.007)\%, \tag{2.26}$$

$$\mathrm{BR}(Z \to \tau^- \tau^+) = (3.370 \pm 0.008)\% \tag{2.27}$$

$$\mathrm{BR}(Z \to e^\mp \mu^\pm) \lesssim 7.5 \times 10^{-7}\,, \tag{2.28}$$

$$\mathrm{BR}(Z \to e^\mp \tau^\pm) \lesssim 9.8 \times 10^{-6} \tag{2.29}$$

$$\mathrm{BR}(Z \to \tau^\mp \mu^\pm) \lesssim 1.2 \times 10^{-5}. \tag{2.30}$$

They will be improved by future experiments Giga-Z, ILC, and CEPC. The model prediction for the branching fraction is

$$\mathrm{BR}(Z \to \ell_i^- \ell_j^+) = \frac{\Gamma(Z \to \ell_i^- \ell_j^+)}{\Gamma_{\rm tot}} = \frac{m_Z}{24\pi\,\Gamma_{\rm tot}}(|\Gamma_{L_{ij}}|^2 + |\Gamma_{R_{ij}}|^2)\,, \tag{2.31}$$

$$\Gamma_{L_{ij}} \approx \frac{g_2}{c_w}\left(-\frac{1}{2} + s_w^2\right)\left[\delta_{ij} + \sum_{a=1-3} \frac{y_{\eta_{ia}} y^\dagger_{\eta_{aj}}}{(4\pi)^2} G(M_{N_a}, m^\pm_{H_2})\right]\,, \tag{2.32}$$

$$\Gamma_{R_{ij}} \approx \frac{g_2 s_w^2}{c_w}\left[\delta_{ij} + \sum_{a=1-3} \frac{y^\dagger_{\chi_{ia}} y_{\chi_{aj}}}{(4\pi)^2} G(M_{N_a}, m^\pm_{H_1})\right], \tag{2.33}$$

where we have neglected terms proportional to s_α^2 and/or $(m_\ell/m_Z)^2$, $\Gamma_{\rm tot} \approx (2.4952 \pm 0.0023)$ GeV, and defined [49]

$$G(m_a, m_b) \approx \frac{m_a^4 - 4m_a^2 m_b^2 + 3m_b^4 - 4m_a^4 \ln[m_a] + 8m_a^2 m_b^2 \ln[m_a] - 4m_b^4 \ln[m_b]}{4(m_a^2 - m_b^2)^2}\,.$$

They are constrained by Eqs. (2.25) −(2.30).

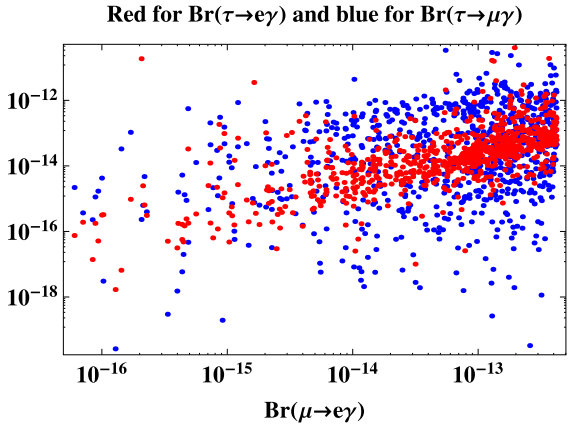

Fig. 4. Scatter plots of BR($\tau \to e\gamma$) (red) and BR($\tau \to \mu\gamma$) (blue) in terms of BR($\mu \to e\gamma$). (For interpretation of the colors in the figure(s), the reader is referred to the web version of this article.)

3. Numerical analysis

For the numerical analysis, we generate input parameters randomly in the following ranges:

$$\begin{aligned}
&(y_{N_{ij}}, |y_\chi|) \in [10^{-8}, 0.1],\ \theta_{1,2,3} \in [10^{-3}i, 2\pi + 100i],\\
&s_\alpha \in [10^{-5}, 10^{-3}],\ s_\beta \in [-1, 1],\\
&(\mu, \mu_\chi, \mu_{\eta\chi}) \in [10^3]\ \text{GeV},\ m_{H^\pm_{1,2}} \in [80, 10^3]\ \text{GeV},\\
&(m_{H_2}, M_{N_1}, M_{N_2}, M_{N_3}) \in [200, 10^3]\ \text{GeV},
\end{aligned} \tag{3.1}$$

where $i, j = 1, 2, 3$, y_N is a symmetric matrix, $\theta_{1,2,3}$ are arbitrary complex values in the Casas-Ibarra parametrization. We fixed $m_{H_1} = m_\phi/2$. The lower bound on $H^\pm_{1,2}$, 80 GeV, comes from the LEP experiment [46,54]. In addition, the LHC gives a mass bound for the charged boson. Especially, the $SU(2)_L$ originated charged boson would have a feature similar to the slepton in the supersymmetric model, since it decays into a charged lepton and missing energy. The lower bound of the mass from the CMS collaboration is 450 GeV [55]. Hence we might apply this bound for our case, although the detail analysis is beyond our scope of this paper. Notice here y_η should satisfy the perturbative limit; $y_\eta \lesssim \sqrt{4\pi}$.

In Fig. 4, we show scatter plots BR($\tau \to e\gamma$) (red) and BR($\tau \to \mu\gamma$) (blue) as a function of BR($\mu \to e\gamma$). It suggests that BR($\tau \to e\gamma$) and BR($\tau \to \mu\gamma$) are much less than the upper bounds of experiments, while the maximum value of BR($\mu \to e\gamma$) reaches the experimental upper bound. In Fig. 5, we show scatter plots of BR($Z \to e\tau$) (red) and BR($Z \to \mu\tau$) (blue) as a function of BR($Z \to e\mu$). It suggests that BR($Z \to e\tau$) and BR($Z \to \mu\tau$) are much less than the upper bounds of experiments, while the maximum value of BR($Z \to e\mu$) is close to the experimental upper bound. Thus BR($Z \to e\mu$) could be tested in the future experiments. As for muon $g-2$, the maximum value is at most 5×10^{-15}, which is much smaller than the current discrepancy. This is because the positive contribution comes from the mixing term between y_η and y_χ only.

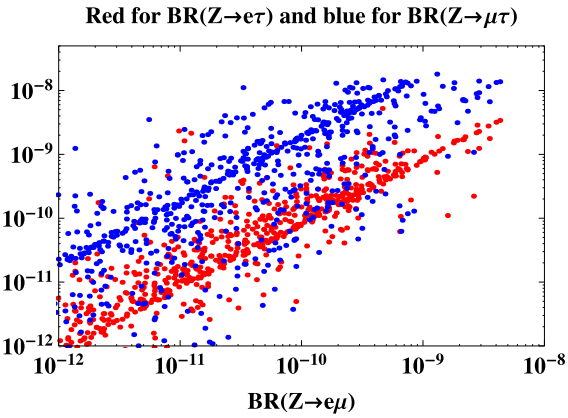

Fig. 5. Scatter plots of BR($Z \to e\tau$) (red) and BR($Z \to \mu\tau$) (blue) in terms of BR($Z \to e\mu$).

4. Summaries and discussions

We have explored the possibility to explain bosonic dark matter candidate with a gauge singlet inside the loop to generate the neutrino mass matrix at two-loop level. Here, our setup is the Zee-Babu type scenario with Z_3 discrete symmetry, in which we have considered the neutrino oscillation data, DM, and lepton flavor violations.

First of all, we have found the upper bound on s_α to be of the order 10^{-2} from the direct detection experiment. Thus the only solution to satisfy the observed relic density is to use the SM Higgs resonance with the DM mass around the half of the Higgs mass, $m_{H_1} \approx m_\phi/2$.

Second, the neutrino mass matrix is reduced by not only the two-loop suppression but also $s_\alpha^2 \approx 10^{-3}$ suppression that comes from the direct detection bound of the DM. As a result, the scale of the neutrino masses is equivalent to that of the three-loop neutrino model.

We have found that the positive muon $g-2$ thanks to $\chi^\pm$. But its typical value $\mathcal{O}(10^{-14})$ in our global analysis is too small to explain the $\sim 3\sigma$ discrepancy of the muon $g-2$ between the experiment and the SM.

We briefly mention the possibility to detect our new particles at the LHC or the ILC. In these kinds of radiative seesaw models, they tend to have large Yukawa couplings in the lepton sector. Therefore, the effect of LFV processes can be large. On the other hand, the bounds from the LHC experiments are typically weaker than the LFV constraints, since new scalar bosons do not couple to quarks. Hence, in this paper we consider only LFV effects.

Acknowledgements

This work was supported in part by the National Research Foundation of Korea (NRF) grant funded by the Korea government (MSIT), Grant No. NRF-2018R1A2A3075605 (S.B.). H. O. is sincerely grateful for all the KIAS members in Korea. This research is supported by the Ministry of Science, ICT and Future Planning, Gyeongsangbuk-do and Pohang City (H.O.). The work was supported from European Regional Development Fund-Project Engineering Applications of Microworld Physics (No. CZ.02.1.01/0.0/0.0/16-019/0000766) (Y.O.).

Appendix A. Cholesky decomposition

A symmetric matrix M can be factorized by Cholesky decomposition. The decomposition is as follows:

$$M = \begin{bmatrix} m_{11} & m_{12} & m_{13} \\ m_{12} & m_{22} & m_{23} \\ m_{13} & m_{23} & m_{33} \end{bmatrix} = LL^T, \tag{A.1}$$

where L is a lower triangular matrix. The explicit form for the matrix L is

$$L = \begin{bmatrix} l_{11} & 0 & 0 \\ l_{21} & l_{22} & 0 \\ l_{31} & l_{32} & l_{33} \end{bmatrix}, \tag{A.2}$$

$$l_{11} = \pm\sqrt{m_{11}}, \tag{A.3}$$

$$l_{21} = \frac{m_{12}}{l_{11}}, \tag{A.4}$$

$$l_{22} = \pm\sqrt{m_{22} - l_{21}^2}, \tag{A.5}$$

$$l_{31} = \frac{m_{13}}{l_{11}}, \tag{A.6}$$

$$l_{32} = \frac{m_{32} - l_{31}l_{21}}{l_{22}}, \tag{A.7}$$

$$l_{33} = \pm\sqrt{m_{33} - l_{31}^2 - l_{32}^2}, \tag{A.8}$$

where we assumed all parameters to be real and positive.

References

[1] A. Zee, Nucl. Phys. B 264 (1986) 99;
K.S. Babu, Phys. Lett. B 203 (1988) 132.
[2] K.S. Babu, C. Macesanu, Phys. Rev. D 67 (2003) 073010, arXiv:hep-ph/0212058.
[3] D. Aristizabal Sierra, M. Hirsch, J. High Energy Phys. 0612 (2006) 052, arXiv:hep-ph/0609307.
[4] M. Nebot, J.F. Oliver, D. Palao, A. Santamaria, Phys. Rev. D 77 (2008) 093013, arXiv:0711.0483 [hep-ph].
[5] D. Schmidt, T. Schwetz, H. Zhang, Nucl. Phys. B 885 (2014) 524, arXiv:1402.2251 [hep-ph].
[6] J. Herrero-Garcia, M. Nebot, N. Rius, A. Santamaria, Nucl. Phys. B 885 (2014) 542, arXiv:1402.4491 [hep-ph].
[7] H.N. Long, V.V. Vien, Int. J. Mod. Phys. A 29 (13) (2014) 1450072, arXiv:1405.1622 [hep-ph].
[8] V. Van Vien, H.N. Long, P.N. Thu, arXiv:1407.8286 [hep-ph].
[9] M. Aoki, S. Kanemura, T. Shindou, K. Yagyu, J. High Energy Phys. 1007 (2010) 084;
M. Aoki, S. Kanemura, T. Shindou, K. Yagyu, J. High Energy Phys. 1011 (2010) 049 (Erratum), arXiv:1005.5159 [hep-ph].
[10] M. Lindner, D. Schmidt, T. Schwetz, Phys. Lett. B 705 (2011) 324, arXiv:1105.4626 [hep-ph].
[11] S. Baek, P. Ko, H. Okada, E. Senaha, J. High Energy Phys. 1409 (2014) 153, arXiv:1209.1685 [hep-ph].
[12] M. Aoki, J. Kubo, H. Takano, Phys. Rev. D 87 (11) (2013) 116001, arXiv:1302.3936 [hep-ph].
[13] Y. Kajiyama, H. Okada, K. Yagyu, Nucl. Phys. B 874 (2013) 198, arXiv:1303.3463 [hep-ph].
[14] Y. Kajiyama, H. Okada, T. Toma, Phys. Rev. D 88 (2013) 015029, arXiv:1303.7356.
[15] S. Baek, H. Okada, T. Toma, J. Cosmol. Astropart. Phys. 1406 (2014) 027, arXiv:1312.3761 [hep-ph].
[16] H. Okada, arXiv:1404.0280 [hep-ph].
[17] H. Okada, T. Toma, K. Yagyu, Phys. Rev. D 90 (9) (2014) 095005, arXiv:1408.0961 [hep-ph].
[18] H. Okada, arXiv:1503.04557 [hep-ph].
[19] C.Q. Geng, L.H. Tsai, arXiv:1503.06987 [hep-ph].

[20] S. Kashiwase, H. Okada, Y. Orikasa, T. Toma, Int. J. Mod. Phys. A 31 (20n21) (2016) 1650121, https://doi.org/10.1142/S0217751X16501219, arXiv:1505.04665 [hep-ph].
[21] M. Aoki, T. Toma, J. Cosmol. Astropart. Phys. 1409 (2014) 016, arXiv:1405.5870 [hep-ph].
[22] S. Baek, H. Okada, T. Toma, Phys. Lett. B 732 (2014) 85, arXiv:1401.6921 [hep-ph].
[23] H. Okada, Y. Orikasa, Phys. Rev. D 93 (1) (2016) 013008, https://doi.org/10.1103/PhysRevD.93.013008, arXiv:1509.04068 [hep-ph].
[24] D. Aristizabal Sierra, A. Degee, L. Dorame, M. Hirsch, J. High Energy Phys. 1503 (2015) 040, arXiv:1411.7038 [hep-ph].
[25] T. Nomura, H. Okada, Phys. Lett. B 756 (2016) 295, arXiv:1601.07339 [hep-ph].
[26] T. Nomura, H. Okada, Y. Orikasa, arXiv:1602.08302 [hep-ph].
[27] C. Bonilla, E. Ma, E. Peinado, J.W.F. Valle, arXiv:1607.03931 [hep-ph].
[28] M. Kohda, H. Sugiyama, K. Tsumura, Phys. Lett. B 718 (2013) 1436, arXiv:1210.5622 [hep-ph].
[29] B. Dasgupta, E. Ma, K. Tsumura, Phys. Rev. D 89 (2014) 041702, arXiv:1308.4138 [hep-ph].
[30] S. Baek, J. High Energy Phys. 1508 (2015) 023, https://doi.org/10.1007/JHEP08(2015)023, arXiv:1410.1992 [hep-ph].
[31] T. Nomura, H. Okada, Phys. Rev. D 94 (2016) 075021, https://doi.org/10.1103/PhysRevD.94.075021, arXiv:1607.04952 [hep-ph].
[32] T. Nomura, H. Okada, arXiv:1609.01504 [hep-ph].
[33] T. Nomura, H. Okada, Y. Orikasa, Phys. Rev. D 94 (11) (2016) 115018, https://doi.org/10.1103/PhysRevD.94.115018, arXiv:1610.04729 [hep-ph].
[34] Z. Liu, P.H. Gu, arXiv:1611.02094 [hep-ph].
[35] R.J. Barlow, Nucl. Phys. B, Proc. Suppl. 218 (2011) 44, https://doi.org/10.1016/j.nuclphysbps.2011.06.009.
[36] D.S. Akerib, et al., arXiv:1608.07648 [astro-ph.CO].
[37] J.M. Cline, K. Kainulainen, P. Scott, C. Weniger, Phys. Rev. D 88 (2013) 055025, https://doi.org/10.1103/PhysRevD.88.055025, arXiv:1306.4710 [hep-ph], Erratum: Phys. Rev. D 92 (3) (2015) 039906, https://doi.org/10.1103/PhysRevD.92.039906.
[38] T. Hambye, F.-S. Ling, L. Lopez Honorez, J. Rocher, J. High Energy Phys. 0907 (2009) 090, https://doi.org/10.1088/1126-6708/2009/07/090, arXiv:0903.4010 [hep-ph], Erratum: J. High Energy Phys. 1005 (2010) 066, https://doi.org/10.1007/JHEP05(2010)066.
[39] S. Kanemura, S. Matsumoto, T. Nabeshima, N. Okada, Phys. Rev. D 82 (2010) 055026, https://doi.org/10.1103/PhysRevD.82.055026, arXiv:1005.5651 [hep-ph].
[40] Z. Maki, M. Nakagawa, S. Sakata, Prog. Theor. Phys. 28 (1962) 870, https://doi.org/10.1143/PTP.28.870.
[41] D.V. Forero, M. Tortola, J.W.F. Valle, Phys. Rev. D 90 (9) (2014) 093006, https://doi.org/10.1103/PhysRevD.90.093006, arXiv:1405.7540 [hep-ph].
[42] N. Aghanim, et al., Planck Collaboration, arXiv:1807.06209 [astro-ph.CO].
[43] T. Toma, A. Vicente, J. High Energy Phys. 1401 (2014) 160, https://doi.org/10.1007/JHEP01(2014)160, arXiv:1312.2840 [hep-ph].
[44] M. Lindner, M. Platscher, F.S. Queiroz, arXiv:1610.06587 [hep-ph].
[45] C. Guo, S.Y. Guo, Z.L. Han, B. Li, Y. Liao, arXiv:1701.02463 [hep-ph].
[46] C. Patrignani, et al., Particle Data Group, Chin. Phys. C 40 (10) (2016) 100001;
M. Tanabashi, et al., Particle Data Group, Phys. Rev. D 98 (3) (2018) 030001, https://doi.org/10.1103/PhysRevD.98.030001.
[47] A.M. Baldini, et al., MEG Collaboration, Eur. Phys. J. C 76 (8) (2016) 434, arXiv:1605.05081 [hep-ex].
[48] K.A. Olive, et al., Particle Data Group, Chin. Phys. C 38 (2014) 090001.
[49] P.J. Mohr, D.B. Newell, B.N. Taylor, Rev. Mod. Phys. 88 (3) (2016) 035009, https://doi.org/10.1103/RevModPhys.88.035009, arXiv:1507.07956 [physics.atom-ph].
[50] E.V. Hungerford, COMET Collaboration, AIP Conf. Proc. 1182 (2009) 694.
[51] C. Dohmen, et al., SINDRUM II Collaboration, Phys. Lett. B 317 (1993) 631.
[52] W.H. Bertl, et al., SINDRUM II Collaboration, Eur. Phys. J. C 47 (2006) 337.
[53] W. Honecker, et al., SINDRUM II Collaboration, Phys. Rev. Lett. 76 (1996) 200.
[54] R. Barate, et al., ALEPH and DELPHI and L3 and OPAL Collaborations and LEP Working Group for Higgs boson searches, Phys. Lett. B 565 (2003) 61, https://doi.org/10.1016/S0370-2693(03)00614-2, arXiv:hep-ex/0306033.
[55] A.M. Sirunyan, et al., CMS Collaboration, arXiv:1806.05264 [hep-ex].